Dynamics of copropagating edge states in a multichannel Mach-Zender interferometer

IOP Conf. Series: Journal of Physics: Conf. Series **906** (2017) 012027 doi:10.1088/1742-6596/906/1/012027

Dynamics of copropagating edge states in a multichannel Mach-Zender interferometer

L. Bellentani[1], A. Beggi[1], P. Bordone[1,2], A. Bertoni[2]

[1]Dipartimento di Scienze Fisiche, Informatiche, Matematiche
Universitá degli studi di Modena e Reggio Emilia, via Campi 213/A 41125 Modena, Italy
[2]CNR-Istituto Nanoscienze, Modena, Italy

E-mail: laura.bellentani@unimore.it

Abstract. We study numerically a multichannel electronic Mach-Zender interferometer, where an orthogonal magnetic field produces edge states. Our time-dependent model is based on the split-step Fourier method and describes the charge carrier as a Gaussian wavepacket of edge states, whose path is defined by split-gate induced potential profiles on the 2DEG at filling factor $\nu = 2$. We analyse a beam splitter with $\sim 50\%$ inter-channel mixing and obtain Aharonov-Bohm oscillations in the transmission probability of the second channel.

1. Introduction

Topologically protected edge states (ES) in the quantum Hall regime are able, in principle, to encode and process quantum information via electron quantum optics devices [1, 2, 3]. The realization of such semiconductor quantum logic gates requires suitable electrostatic potential profiles for the dynamical control of flying qubits, which is the target of our work.
In detail, we model a multichannel Mach-Zender interferometer (MZI) with bulk filling factor $\nu = 2$ [1, 4], where two parallel spin-degenerate edge states are forced to follow different paths. In contrast to the Corbino interferometer [3], we adopt the geometry proposed in Ref.[4], which allows concatenation in series and a smaller loop area, therefore reducing the effect of phase averaging. Instead of simulating delocalized plane-waves, we study the single-particle dynamical properties of the MZI describing the travelling charge as a strongly localized wavepacket (WP) of edge states [5, 6]. In analogy to the single channel MZI [7], our results focus on the measurement of Aharonov-Bohm (AB) oscillations, comparing numerical data to a simplified analytical model.

2. Physical system

Our model describes a 2DEG on the x-y plane, where the integer quantum Hall effect is generated by a uniform and orthogonal magnetic field B. A local confining potential $V(x)$ - constituting the edges of the MZI - is introduced to form edge states, chiral and quasi-adiabatic channels following the boundary between low-potential and high-potential regions of the device. With these assumptions, neglecting electron-electron interaction, the wavefunction of the single-particle Hamiltonian can be rewritten as $\Psi_n(x, y, k) = \phi_{n,k}(x)e^{iky}$. The exponential factor e^{iky} defines a travelling state along the y direction with momentum k, while $\phi_{n,k}(x)$ is the eigenstate of the 1D effective Hamiltonian with energy E_n at fixed k.

The study of dynamical properties in our time-dependent approach requires the description of the electronic state with a localized wavefunction. Therefore, the ESs are combined with Gaussian weights $F_\sigma(k) = \sqrt{\sigma}(2\pi)^{\frac{-3}{4}} e^{-\sigma^2(k-k_0)^2} e^{-iky_0}$ in the function $\Psi^o_n(x,y) = \int dk F_\sigma(k)\phi_{n,k}(x)e^{iky}$, which represents a minimum-uncertainty initial state localized at $(x_0 = -\hbar k_0/eB, y_0)$ with group velocity $v_g = \hbar k_0/m^*$.

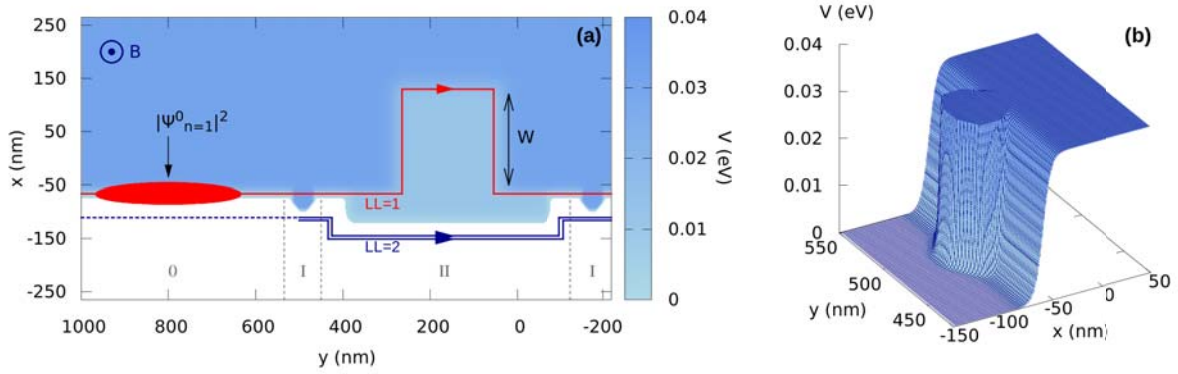

Figure 1. The two-channel MZI device. **a)**Top view of the device with the intended path of the two channels (single line for n=1 and double line for n=2) and initial electronic density probability ($|\Psi^0_{n=1}|^2$). Region *0*: injection; Region *I*: beam splitters; Region *II*: step potential. **b)** Potential profile adopted for the beam splitter.

After the injection region, where the potential varies only along x, V presents also a dependence on y [4]. Specifically, the paths of the ESs, together with two BSs, form a MZI. In order to mimic the smooth potential induced by realistic split gates, we adopt a Fermi-function shape for the transition between regions with different potential (i.e. at different filling factor). In contrast to our previous work [7], a bulk filling factor $\nu = 2$ characterizes the low-potential region, where the first two Landau levels ($n = 1, 2$) are available.
The complete device is plotted in Fig.1(a). Firstly, the wavepacket (initialized in $n = 1$) impinges on the beam splitter (BS) modeled with the sharp potential dip reported in Fig.1(b). Here, the scattering process coherently mixes the wavefunction in the two copropagating channels with different index n. Then, a suitable potential profile forces a different path for the two channels and the accumulation of a relative phase. Finally, the two parts of the wavefunction are recollected on a second beam splitter, where they interfere. At the end of the MZI the selective measurement of the transmission probability is performed through an additional mesa and an imaginary potential, which adsorbs only the channel with $n = 1$. Consequently, the norm of the final wavefunction coincides with the total transmission probability P_{21} from the first to the second channel, whose amplitude shows the characteristic oscillations induced by the interference.

3. Numerical simulations

In order to analyse the particle dynamics, we solve the time-dependent Schrödinger equation with the split-step Fourier method [7], using a time step $\delta t = 10^{-16}s$. The Gaussian WP of ESs is initialized in $n = 1$, $\sigma = 60nm$ and $k_0 = -0.387nm^{-1}$.

As a first step, we define a proper geometry of the potential $V(x, y)$ to obtain the BS. Following Ref.[4, 8, 9], such gate can be represented by a sharp potential profile, which splits elastically the incoming wave in the first two Landau levels. Indeed, the scattering redistributes the k components of the wavepacket in the available states, with a probability measured by the

transmission coefficient $t_{f,i}^{BS}$ (i=1,2 for the initial state and f=1,2 for the final one). Such a parameter can be controlled by tuning the energy composition of the wavepacket, the magnetic field intensity B and the shape of the potential barrier. Regarding the sharpness of the local potential, numerical calculations [8] show indeed that spatial inhomogeneities on a scale smaller than the magnetic length are required to split efficiently the impinging state. After testing various potential profiles, we achieve a $t_{2,1}^{BS}$ coefficient of $(50 \pm 1)\%$ with the shape plotted in Fig.1(b), at B=5T. We simulate the scattering of the initial WP in both the first and the second Landau level, with essentially symmetric results. Moreover, we extracted the energy dependence of the transmission coefficients t_{fi}^{BS}, observing a quasi-flat dispersion in our energy bias, which ensures a coherent 50% mixing of the two channels without the resonant condition [10].

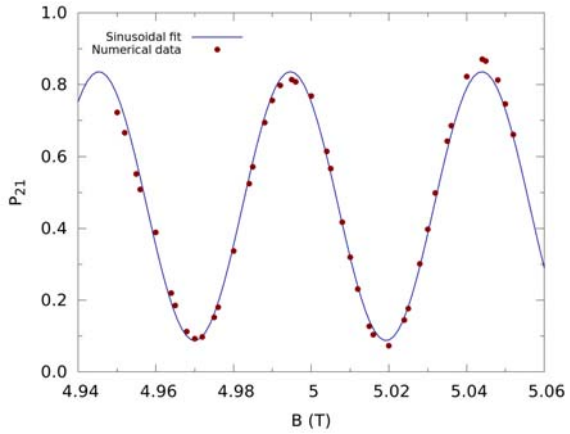

Figure 2. Transmission probability from $n = 1$ to $n = 2$ at the end of the device as a function of B simulated numerically (dots) and fit with eq.(1) (solid line).

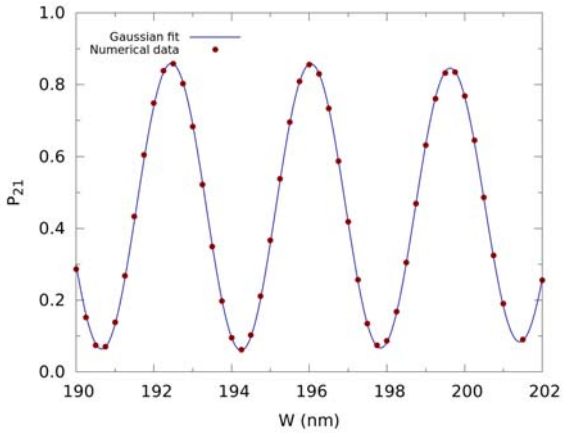

Figure 3. Transmission probability from $n = 1$ to $n = 2$ at the end of the device as a function of W simulated numerically (dots) and fit with eq.(2) (solid line).

Once the coherent superposition is realized, the mesa in Fig.1(a) splits the beam in two parts following different paths. Indeed, such potential step shifts upwards the band structure [4], forcing the two Landau levels to be filled at different wavevectors. Considering the relation $x = -\frac{\hbar k}{eB}$, this implies a different localization of the two channels in the x direction. Therefore, the two paths can be tuned by reshaping the local potential, and a length mismatch introduces a phase difference. To this aim, we design a step potential with smooth edges and avoid an undesired additional inter-channel mixing. Furthermore, our time-dependent approach entails a particular attention to the shape of the mesa. Indeed, this must ensure the simultaneous recollection of the two localized wavepackets at the second beam splitter, taking into account the different group velocities.

Table 1. Parameters for the transmission probability $P_{21}(W)$: a) from a fit of numerical simulation with eq.(2) and b) from the analytical model.

	A	A_0	ν_{21}	k_x (nm^{-1})	Σ (nm)
a)Fit of simulations	0.400±0.004	0.460±0.002	0.87	1.750	21.7±0.5
b)Analytical model	0.5	0.5	1	1.9	18.3

4. Results and discussion

We simulate the interference process varying both the magnetic field intensity and the length mismatch of the two paths at the mesa. We obtain AB oscillation of the transmission probability P_{21}, plotted in Fig.2 and Fig.3 for a variation of B and W (width of the mesa in Fig.1(a)) respectively. The numerical results are fit by the following functions:

$$P_{21}(B) = A_0 + Ae^{(-\frac{(W-W_0)^2}{2\Sigma^2})} cos(k_B B + \Phi_1), \quad (1)$$

$$P_{21}(W) = A_0 + Ae^{(-\frac{(W-W_0)^2}{2\Sigma^2})} \cos(k_x W + \Phi_0), \quad (2)$$

which describe the total transmission probability in our MZI for the initial Gaussian WP of ESs previously described. The results of the Gaussian fit in eq.(2) are finally compared to the predictions of our simplified theoretical model [7] in Tab.1.

Concerning the magnetically-driven interference, we observe that the oscillations do not form a perfect sinusoid, but the amplitude slightly increases with the magnetic field intensity. We relate this feature to the actual magnetic dependence of the scattering at the BS and at the mesa. Indeed, we must stress that eq.(1)-(2) are calculated assuming $t_{1,2}^{BS} = 0.5$, without including the dependence on energy and B. On the other hand, in Fig.3 the variation of the oscillation amplitude is induced by the Gaussian shape of the wavefunction, which is a unique feature of the time-dependent approach. In detail, when the length mismatch between the two paths approaches σ, the overlap between the two wavefunctions is reduced and the oscillation amplitude becomes weaker [11]. Moreover, in contrast to theoretical predictions, we achieve a maximum visibility $\nu_2^{max} \approx 87\%$ in place of unity. Different factors contribute to this reduction. Firstly, our theoretical model neglects the energy dependence of the dynamic phase and transmission amplitudes, assuming the impinging wavefunction equally scattered in the two available states. Additionally, despite its smoothness, the step potential induces a small inter-channel mixing (around 2%), which could be eventually reduced by shifting upwards the height of the mesa or increasing the smoothness of the barrier. Finally, we neglect the partial filling of the third Landau level, which is an available state in the selected energy bias.

In conclusion, we showed that the oscillating transmission of a two channel MZI with realistic dimensions can be obtained by solving numerically the time-dependent Schrödinger equation with the corresponding potential landscape. We showed how specific features of the transmission characteristic are linked to the localization of the propagating carrier. Our single-particle simulations validate this system for the implementation of single-qubit logic gates, and, in perspective, the simulation of two interacting carriers should expose its ability to create two-qubits gates.

References

[1] Neder I, Heiblum M, Mahalu D, and Umansky V 2007 *Phys. Rev. Lett.* **98** 036803
[2] Roddaro S, Chirolli L, Taddei F, Polini M and Giovannetti V 2013 *Phys. Rev.* B **87** 075321
[3] Deviatov E V 2013 *AIP Low. Temp. Phys* **39** 7
[4] Giovannetti V, Taddei F, Frustaglia D, and Fazio R 2008 *Phys. Rev.* B **77** 155320
[5] Gaury B, Weston J and Waintal X 2014 *Phys. Rev.* B **90** 161305
[6] Kataoka M, Johnson N, Emary C, See P, Griffiths J P, Jones G A C, Farrer I, Ritchie D A, Pepper M and Janssen T J B M 2016 *Phys. Rev. Lett* **116** 126803
[7] Beggi A, Bordone P, Buscemi F and Bertoni A 2015 *J. Phys.: Cond. Matt.* **27** 475301
[8] Palacios J J and Tejedor C 1991 *Phys. Rev.* B **45** 9059
[9] Paradiso N, Heun S, Roddaro S, Venturelli D, Taddei F, Giovannetti V, Fazio R, Biasiol G, Sorba L, and Beltram F 2011 *Phys. Rev.* B **83** 155305
[10] Karmakar B, Venturelli D, Chirolli L, Giovannetti V, Fazio R, Roddaro S, Pfeiffer L N, West K W, Taddei F, and Pellegrin V 2015 *Phys. Rev* B **92** 195303
[11] Haack G, Moskalets M, Splettstoesser J and Buttiker M 2011 *Phys. Rev.* B **84** 081303